Available online at www.sciencedirect.com
ScienceDirect
Lithos 103 (2008) 445–465
LITHOS
www.elsevier.com/locate/lithos

Geochemistry of S-type granitic rocks from the reversely zoned Castelo Branco pluton (central Portugal)

I.M.H.R. Antunes [a,*], A.M.R. Neiva [b], M.M.V.G. Silva [b], F. Corfu [c]

[a] Polytechnic Institute of Castelo Branco, 6000-919 Castelo Branco, Portugal
[b] Department of Earth Sciences, University of Coimbra, 3000-272 Coimbra, Portugal
[c] Department of Geosciences, University of Oslo, PB1047 Blindern, N-0316, Norway

Received 8 March 2007; accepted 11 October 2007
Available online 23 October 2007

Abstract

The zoned pluton from Castelo Branco consists of Variscan peraluminous S-type granitic rocks. A muscovite>biotite granite in the pluton's core is surrounded successively by biotite>muscovite granodiorite, porphyritic biotite>muscovite granodiorite grading to biotite=muscovite granite, and finally by muscovite>biotite granite. ID-TIMS U–Pb ages for zircon and monazite indicate that all phases of the pluton formed at 310±1 Ma. Whole-rock analyses show slight variation in $^{87}Sr/^{86}Sr_{310\ Ma}$ between 0.708 and 0.712, $\varepsilon Nd_{310\ Ma}$ values between −1 and −4 and $\delta^{18}O$ values between 12.2 and 13.6. These geological, mineralogical, geochemical and isotopic data indicate a crustal origin of the suite, probably from partial melting of heterogeneous Early Paleozoic pelitic country rock. In detail there is evidence for derivation from different sources, but also fractional crystallization linking some of internal plutonic phases. Least-squares analysis of major elements and modelling of trace elements indicate that the porphyritic granodiorite and biotite=muscovite granite were derived from the granodiorite magma by fractional crystallization of plagioclase, quartz, biotite and ilmenite. By contrast variation diagrams of major and trace elements in biotite and muscovite, the behaviours of Ba in microcline and whole-rock $\delta^{18}O$, the REE patterns of rocks and isotopic data indicate that both muscovite-dominant granites were probably originated by two distinct pulses of granite magma.

Keywords: Reversely zoned pluton; S-type granitic rocks; U–Pb zircon and monazite ages; Isotopic data; Fractional crystallization

1. Introduction

The Central Iberian Zone (CIZ) is the innermost zone of the Iberian Variscan Belt, formed during the collision of Laurentia–Baltica with Gondwana. Like other collisional belts, it is characterized by voluminous granitic magmatism, which produced a wide range of granitoids. Most of them are correlated with the last ductile deformation phase (D3) of Westphalian age (Noronha et al., 1981; Ferreira et al., 1987; Pinto et al., 1987; Dias et al., 1998; Azevedo and Nolan, 1998; Almeida et al., 2002; Valle Aguado et al., 2005). Granitoid plutons in CIZ show a large compositional diversity, from peraluminous to calc-alkaline and subalkaline types (Neiva, 1993; Dias et al., 1998; Silva and Neiva, 1999/2000; Neiva and Gomes, 2001) and some are concentrically zoned.

The normal sequence of zoning in a pluton from the periphery to the core involves an increase in modal

* Corresponding author. Tel.: +351 272339900; fax: +351 272339901.
E-mail address: imantunes@esa.ipcb.pt (I.M.H.R. Antunes).

0024-4937/$ - see front matter © 2007 Elsevier B.V. All rights reserved.
doi:10.1016/j.lithos.2007.10.003

quartz and potassium feldspar and a decrease in mafic minerals and in the An content of plagioclase (e.g., Pitcher, 1997; El-Nisr and El-Sayed, 2002). Reversely zoned plutons have a more felsic rim and a more mafic core and are rare (e.g., Allen, 1992; Barbey et al., 2001). In situ fractional crystallization through sidewall crystallization and solidification is the most invoked process for "normally" zoned plutons as the minerals with the highest crystallization temperatures reside in the rim of the pluton (e.g., Allen, 1992; Neiva and Campos, 1992; Pitcher, 1997; El-Nisr and El-Sayed, 2002; Vigneresse, 2004; Gomes and Neiva, 2005). Different mechanisms are invoked to explain the reversely zoned plutons. In situ crystallization, either from the wall rocks inwards with concentration of mafic minerals toward the core by flow segregation with progressive solidification of magma chamber, or from the core outwards, due to volatile enrichment and depression of the liquidus temperature in magmas close to the walls, as the pluton apparently cooled from the core to the periphery are two mechanisms that imply compositional variation at or near the level of exposure (Allen, 1992). The reordering of an underlying, vertically stratified, magma chamber either by intrusion through an orifice or by emplacement of composite diapirs, which can be caused by magma mixing and minor fractional crystallization, are two models that imply the occurrence of a layered magma chamber at depth reorganised through intrusions to a higher level (Allen, 1992). Fractional crystallization accompanied by contamination of crustal material mainly before emplacement has been invoked to explain a reversely S-type zoned pluton from Morocco (Barbey et al., 2001). Zoning is more visible in I-type granites, while in S-type granites it can be due to differences in the composition of the metapelitic source that partially melted (e.g., Pitcher, 1997).

The Castelo Branco pluton is a composite and zoned intrusion of peraluminous (S-type) affinity. It is intrusive at a higher level than the source area, emplaced in an epizonal domain and late-tectonic. It contains five granitoid units forming a roughly circular body. This paper reports its petrographic, mineralogical, geochemical and isotopic (Rb/Sr, Sm/Nd, $\delta^{18}O$, U–Pb) characteristics. The aim of the study was to date the Castelo Branco pluton and to understand the processes responsible for its compositional variability.

2. Geology

The Castelo Branco pluton is located within the Central Iberian Zone (CIZ) of the Iberian Massif, which is one of the largest segments of the European Variscan fold belt. The CIZ granitoids have been emplaced mainly during and after the ductile deformation phase D3 of Namurian–Westphalian age. They are classified according to their emplacement ages as syn-D3, late-D3, late- to post-D3 and post-D3 (Ferreira et al., 1987; Dias et al., 1998) and syntectonic to late-tectonic (336–304 Ma) and post-tectonic (300–280 Ma) granites (Neiva and Gomes, 2001).

The Castelo Branco pluton is exposed over an area of 390 km^2, with a mean diameter of 19 km, and consists of five concentric late-tectonic Variscan granitic bodies, which intruded the Cambrian schist–metagraywacke complex and also a medium-grained biotite granodiorite of 480±2 Ma (zircon U–Pb age; Antunes, 2006) in the NE (Fig. 1). A medium- to fine-grained muscovite>biotite granite (G1) forms the pluton's core and is surrounded by medium- to fine-grained slightly porphyritic biotite> muscovite granodiorite (G2), encircled by, and grading to medium- to coarse-grained porphyritic biotite>muscovite granodiorite (G3), grading into a medium- to coarse-grained porphyritic biotite=muscovite granite (G4), which contains equal amounts of biotite and muscovite. Granodiorite G3 and granite G4 contain rounded enclaves of granodiorite G2. A coarse-grained muscovite>biotite granite (G5) occupies the periphery of the pluton in the sector from N to E. The contact between granite G1 and granodiorite G2 is sharp. The contact between granites G4 and G5 is also sharp, but the two granites are usually altered at this contact.

A metasedimentary xenolith of 12.5×8.0 cm was found in granite G4. Surmicaceous enclaves were found in all granitic rocks, except G5. They are common in granodiorite G2 and granite G4, scarce in granite G1 and rare in granodiorite G3. They range from 0.5×0.4 cm to 2.4×1.3 cm, but the biggest is 4.3×1.9 cm and occurs in G2.

The schist–metagraywacke complex and the granitic rocks are cut by aplite-pegmatite dykes and quartz veins.

This pluton generated a contact metamorphic aureole up to 2 km wide, into which metasediments recrystallized as pelitic hornfels in the inner zone, and as micaschists in the outer zone.

3. Petrography

The granitic rocks from the Castelo Branco pluton contain quartz, microperthitic microcline, plagioclase, biotite, some chlorite, muscovite, tourmaline, monazite, apatite, zircon, ilmenite and rutile. Granodiorite G3 and granite G4 also contain magmatic andalusite, sillimanite and cordierite. Sillimanite also occurs in granodiorite G2. The modal compositions are given in Table 1. They

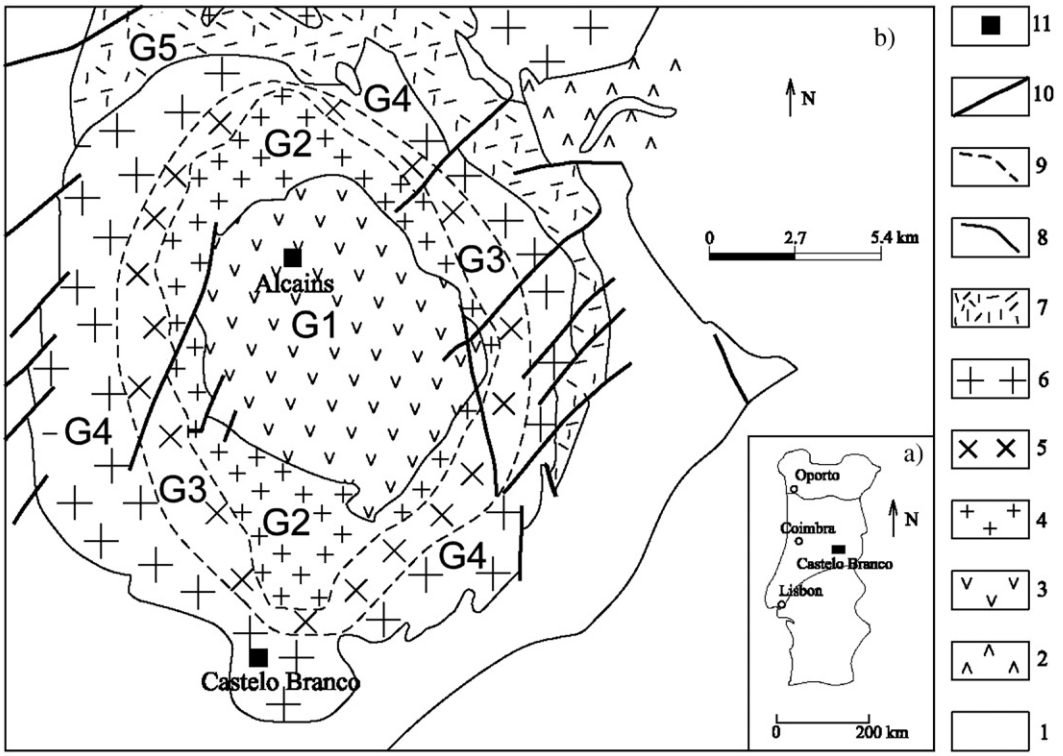

Fig. 1. (a) Location of the Castelo Branco area; (b) Geological map of the Castelo Branco pluton (modified from the Portuguese Geological Survey, 1992). 1 — Cambrian schist–metagraywacke complex, 2 — medium-grained biotite granodiorite, 3 — medium- to fine-grained muscovite>biotite granite (G1), 4 — medium- to fine-grained slightly porphyritic biotite>muscovite granodiorite (G2), 5 — medium- to coarse-grained porphyritic biotite>muscovite granodiorite (G3), 6 — medium- to coarse-grained porphyritic biotite=muscovite granite (G4), 7 — coarse-grained muscovite>biotite granite (G5), 8 — geological contact, 9 — gradational contact, 10 — fault, 11 — town and village.

plot in the granodiorite and monzogranite fields of the QAP diagram (Fig. 2).

Muscovite-dominant granites G1 and G5 have subhedral granular texture, while biotite-dominant granodiorites G2 and G3 and also granite G4 containing similar amounts of biotite and muscovite show a porphyritic subhedral granular texture. Granodiorite G2 contains phenocrysts of microcline (4×1 cm) and granodiorite G3 and granite G4 have phenocrysts of microcline (2×1 cm) and albite–oligoclase (9×4 cm).

Quartz is anhedral to subhedral with undulatory extinction and generally contains inclusions of the other minerals, better shown in the last crystallized quartz generation.

Plagioclase is generally subhedral and polysynthetically twinned. The phenocrystic plagioclase of granodiorite G3 and granite G4 is albite–oligoclase. The matrix plagioclase is albite in granites G1 and G5 and albite–oligoclase in granodiorites G2 and G3 and granite G4. Plagioclase has inclusions of biotite, muscovite, quartz, zircon, monazite, apatite and ilmenite. Plagioclase lamellae, which are about 5 μm thick, in the slightly perthitic microcline, range from An_2 to An_7. Rare mirmekite was found in granite G4.

Microcline is slightly microperthitic and subhedral. Most of the granitic rocks, except granites G1 and G5, have phenocrysts of slightly microperthitic microcline which were formed during the early crystallization. The phenocrysts show better defined cross-hatched twinning than the matrix. Microcline contains inclusions of plagioclase, biotite, muscovite, quartz and apatite.

Biotite is subhedral, dark reddish brown, locally altered to chlorite. Muscovite is also subhedral, often intergrown with biotite and rarely with quartz. The micas host inclusions of zircon, monazite, apatite and ilmenite.

Andalusite occurs in euhedral crystals included in muscovite from granodiorite G3 and granite G4 (Table 1). Sillimanite occurs as needles included in muscovite from granodiorites G2 and G3 and in andalusite and muscovite from granite G4.

Cordierite was only found in granodiorite G3 and granite G4 (Table 1). It occurs as euhedral prismatic crystals partially included in muscovite and generally without inclusions. Some are altered into pinite.

Table 1
Average modal compositions and representative chemical analyses in wt.% and trace elements in ppm of granitic rocks from the Castelo Branco pluton, central Portugal

	G1	G2	G3	G4	G5
Samples	$n=10$	$n=6$	$n=4$	$n=11$	$n=3$
Quartz	30.0	29.3	30.8	32.0	29.8
Plagioclase	27.0	28.3	34.4	28.3	25.1
Microcline	25.3	12.2	13.6	23.9	24.6
Biotite	4.0	17.3	13.1	6.7	3.8
Muscovite	12.6	8.9	4.7	6.6	14.2
Tourmaline	0.4	1.2	0.3	0.3	0.8
Andalusite	–	–	0.8	0.7	–
Cordierite	–	–	0.1	0.6	–
Others	0.7	2.8	2.2	0.9	1.7

	GCL7	GEB2	GIN	INFX2	PC	BCAL	ER	NAC	LARDO	LC1
SiO_2	72.09	73.10	68.78	69.37	70.36	71.52	71.56	72.99	72.90	74.27
TiO_2	0.19	0.16	0.58	0.49	0.39	0.34	0.31	0.22	0.17	0.14
Al_2O_3	14.89	15.12	15.83	15.42	15.42	14.85	15.17	14.75	14.82	14.24
Fe_2O_3	0.12	0.28	0.32	0.08	0.28	0.28	0.01	0.15	0.25	0.29
FeO	1.19	0.82	3.08	2.84	2.34	2.02	1.92	1.61	1.03	0.87
MnO	0.02	0.02	0.05	0.04	0.03	0.04	0.02	0.04	0.02	0.01
MgO	0.45	0.32	1.21	1.03	0.72	0.63	0.57	0.44	0.29	0.22
CaO	0.53	0.46	1.52	1.33	1.01	0.87	0.98	0.65	0.56	0.36
Na_2O	4.03	4.06	3.90	3.88	3.90	4.07	4.00	4.14	3.56	3.50
K_2O	4.88	5.03	4.06	4.28	4.49	4.45	4.99	4.30	4.79	4.47
P_2O_5	0.34	0.38	0.31	0.31	0.36	0.36	0.32	0.39	0.45	0.36
H_2O+	0.85	0.43	0.34	0.64	0.81	0.56	0.56	0.65	0.64	0.78
H_2O-	0.09	0.08	0.03	0.06	0.08	0.05	0.06	0.06	0.06	0.02
Total	99.67	100.26	100.01	99.77	100.19	100.04	100.47	100.39	99.55	99.53
F	1331	892	883	1126	1221	1502	734	2103	1399	1173
Ga	22	22	22	21	23	21	21	24	24	20
Cr	32	19	47	38	28	27	30	31	10	9
W	11	13	12	14	13	14	14	9	3	3
V	13	8	56	46	33	26	30	16	12	6
Nb	9	10	17	14	15	13	12	15	13	13
Sn	15	14	12	12	10	12	8	20	14	13
Zn	67	65	72	63	77	73	64	93	77	74
Li	201	199	141	133	139	164	110	238	203	175
Ni	*	*	12	7	5	4	6	5	5	*
Zr	91	78	238	207	168	148	156	94	81	70
Cu	9	6	14	10	11	4	8	*	8	10
Sc	*	*	9	8	*	6	*	*	*	*
Y	9	6	23	17	17	13	12	9	8	6
Sr	49	42	113	106	74	64	73	37	32	19
Pb	26	28	24	26	23	25	27	20	23	20
Ba	234	194	502	473	337	287	352	144	188	116
Rb	273	275	192	174	222	237	205	309	337	309
Cs	28	34	14	15	18	20	13	25	22	20
U	11	7	7	6	7	10	7	6	7	*
Th	10	4	13	13	9	11	10	7	4	4
As	*	*	*	*	*	12	*	13	*	*

G1 — medium- to fine-grained muscovite>biotite granite, G2 — medium- to fine-grained slightly porphyritic biotite>muscovite granodiorite, G3 — medium- to coarse-grained porphyritic biotite>muscovite granodiorite, G4 — medium- to coarse-grained porphyritic biotite=muscovite granite, G5 — coarse-grained muscovite>biotite granite. *n* — Number of analyzed samples, — not detected, * — below the limit of sensitivity. Analyst: I.M.H.R. Antunes.

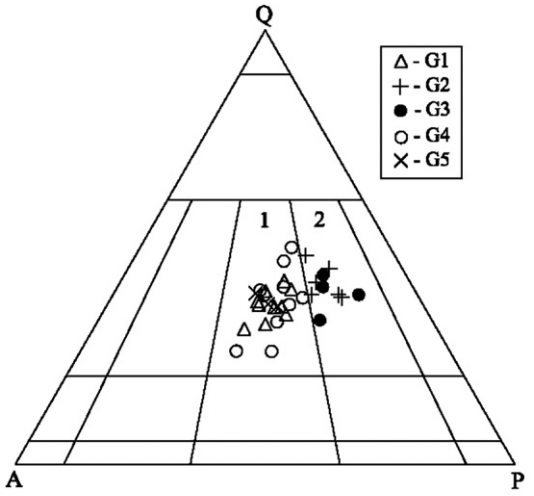

Fig. 2. Q–A–P diagram of Le Bas and Streckeisen (1991) with the granitic rocks from the Castelo Branco pluton. Fields: 1 — monzogranite, 2 — granodiorite. Symbols: △ — medium- to fine-grained muscovite> biotite granite G1; + — medium- to fine-grained slightly porphyritic biotite>muscovite granodiorite G2; ● — medium- to coarse-grained porphyritic biotite>muscovite granodiorite G3; ○ — medium- to coarse-grained porphyritic biotite=muscovite granite G4; × — coarse-grained muscovite>biotite granite G5.

Tourmaline is subhedral to anhedral in unzoned crystals or concentrically zoned crystals which have a small core and a large rim. It contains inclusions of zircon, biotite, ilmenite and apatite. Tourmaline partially replaces micas.

Euhedral zircon, monazite and apatite occur mainly as inclusions in biotite, but also in muscovite and rarely in plagioclase. Apatite is the most abundant accessory mineral occurs as barrels and contains monazite inclusions. Ilmenite occurs mainly included in biotite.

Some alteration effects such as chloritization of biotite and the occurrence of secondary muscovite, particularly replacing plagioclase, were found.

4. Analytical methods

The micas were separated using a magnetic separator and heavy liquids to determine FeO and trace elements. A purity of about 99.8% was estimated by petrographic examination of the powders. The principal contaminants are zircon, monazite and apatite.

The major and trace elements of the granitic rocks were determined by X-ray fluorescence at Southampton Oceanography Centre in Southampton, U.K., with a Philips Magic ProPW 2540 VRC Spectrometer, using the method of Croudace and Thorpe (1988) and Croudace and Gilligan (1990). Precision is ±1% for major elements and ±5% for trace elements.

FeO of granitic rocks and biotites was determined by titration with a standardised potassium permanganate solution; H_2O+ was determined using a Penfield tube. Both had a precision of about ±1%. Li was determined by atomic absorption, while F was determined by selective ion electrode analysis. The precision was about ±2% for both. These determinations were carried out in the Department of Earth Sciences, University of Coimbra.

The rare earth elements of the granitic rocks were determined using a VG Elemental Plasma Quad PQ2+ ICP-MS in liquid mode at Southampton Oceanography Centre in Southampton, U.K. with a precision of ±5%. The trace elements of micas were determined by ICP-MS in liquid mode in the SGS Laboratory, Canada; their precision is ±5%.

Mineral analyses have been determined on a Cameca Camebax SX-50 electron microprobe at the Laboratório de Geologia e Geocronologia dos Serviços Comuns de Investigação of the University of Oviedo, Spain. The analyses were carried out with an accelerating voltage of 15 kV and a beam current of 15 nA. Analyses of micas were obtained on a Jeol JXA-8600 Superprobe with an accelerating voltage of 20 kV and a beam current of 20 nA at the Department of Earth Sciences, University of Bristol, U.K.

The Sr and Nd isotope analyses were obtained at the Centro de Instrumentación Científica of the University of Granada, Spain. Samples were digested using ultra-clean reagents and analyzed by thermal ionization mass spectrometry (TIMS) in a Finnigan Mat 262 spectrometer, after chromatographic separation with ion-exchange resins following the method developed by Montero and Bea (1998). $^{87}Rb/^{86}Sr$ and $^{147}Sm/^{144}Nd$ were determined with a precision better than 1.2% and 0.9% (2σ), respectively. $^{87}Rb/^{86}Sr$ versus $^{87}Sr/^{86}Sr$ regression lines were calculated using the least-squares method of York (1969) as implemented in the Isoplot program (Ludwig, 1999). Errors are quoted at the 95% confidence level and are 2σ.

Oxygen-isotope analyses of whole-rock samples were carried out at the Department of Earth Sciences, the University of Western Ontario, Canada, using a conventional extraction line and employing chlorine trifluoride as the reagent and with a precision of ±0.2‰, using a quartz standard.

Zircon and monazite separation was carried out by a combination of magnetic separation and heavy liquids. Grains were selected by handpicking under a binocular microscope and abraded to remove external disturbed domains (Davis et al., 1982; Krogh, 1982). The U–Pb isotopic results for zircon and monazite were obtained by isotope dilution thermal ionization mass spectrometry

using a Finnigan Mat 262 spectrometer at the Department of Geosciences, University of Oslo, Norway, following the standard procedure of Krogh (1973) with the adaptations described by Corfu and Andersen (2002), Corfu and Evins (2002) and Corfu (2004). The initial Pb correction was done using compositions calculated with the Stacey and Kramers (1975) model. The decay constants used are those of Jaffey et al. (1971). The Isoplot program (Ludwig, 1999) was used for the plots and regression. All uncertainties relative to the analyses and ages are given at the 2σ level.

5. Whole-rock geochemistry

The major, trace and rare earth element contents of granitic rocks from the Castelo Branco pluton are given in Tables 1 and 2. The granitic rocks are peraluminous with a molecular ratio $Al_2O_3/(CaO+Na_2O+K_2O)$ of 1.1 to 1.3. Normative corundum content ranges from 2.7 to 3.8. According to the geochemical classification of Frost et al. (2001), these granitic rocks are mainly magnesian and alkali-calcic.

The variation diagrams for selected major and trace elements and trace/major element ratios of the granitic rocks versus total FeO show curvilinear variation trends, defined by the biotite>muscovite granodiorites G2 and G3, biotite=muscovite granite G4 and muscovite>biotite granite G5 (Fig. 3). The muscovite>biotite granite G1 from the pluton's core does not fit the general trend. Total FeO has been chosen as a differentiation index for the variation diagrams because it shows more variability of the granitic rocks than SiO_2.

The chondrite-normalized REE patterns of G2, G3 G4 are subparallel (Fig. 4). From granodiorite G2 to granite G4, the REE abundances (ΣREE=88.7–192.7) and the light REE (LREE) fractionation with respect to heavy REE (HREE) (18.9–24.9) decrease, while the negative Eu anomaly (Eu/Eu*=0.45–0.61) increases. The pattern of G5 flattens out in the HREE part crossing that of G4 at Ho and that of G1 at Gd.

6. Isotopic data

6.1. ID-TIMS U–Pb results on zircon and monazite

U–Pb isotopic analyses were carried out on zircon and monazite from three samples representing granitic rocks G1, G2 and G5 using the ID-TIMS method (Table 3).

Of the three multi-grain fraction analyses done on G1 zircons, two are discordant (fractions 2 and 3) suggesting the presence of an inherited component (Table 3 and Fig. 5a). The third zircon (fraction 1) analysis of long prisms is concordant yielding a Concordia age of 309.9±1.1 Ma. Two single grain analyses of monazite (fractions 4 and 5) plot slightly reversely discordant, a fact commonly linked to ^{230}Th initial excess, which eventually result in an excess of ^{206}Pb and reverse discordance (Schärer, 1984; Kalt et al., 2000). The ^{207}Pb/^{235}U ratio is not affected by this disequilibrium effect and can be used as the closest estimate for the age of the monazite. For the two monazite analyses of sample G1 this ratio yields an average of 309.5±0.9 Ma, which overlaps the zircon age. Based on these data we conclude that the central granite G1 crystallized at 310±1 Ma.

Three zircon analyses for a sample of granodiorite G2 plot on or close to Concordia (Fig. 5b). The concordant one (fraction 8) defines a Concordia age of 310.1±0.8 Ma.

Table 2
Representative analyses of rare earth elements (ppm) of granitic rocks from the Castelo Branco pluton, central Portugal

	G1		G2		G3		G4		G5	
	GCL7	GEB2	GIN	INFX2	PC	BCAL	ER	NAC	LARDO	LC1
La	13.43	7.54	37.96	37.40	25.59	24.31	19.18	12.55	9.90	7.70
Ce	37.83	24.50	90.16	83.72	58.79	57.19	45.29	32.65	23.60	17.70
Pr	4.15	2.39	9.40	9.16	6.82	6.82	5.40	3.63	2.90	2.31
Nd	16.41	9.42	36.36	37.06	28.82	27.03	22.52	15.11	11.40	8.60
Sm	3.77	2.76	6.59	6.85	5.95	5.44	4.55	3.46	2.80	2.10
Eu	0.41	0.30	1.20	1.20	0.98	0.73	0.71	0.38	0.32	0.22
Gd	2.71	2.30	5.03	4.99	4.86	3.88	3.35	2.56	2.46	1.77
Tb	0.35	0.30	0.68	0.70	0.69	0.55	0.48	0.38	0.40	0.26
Dy	1.44	1.24	3.50	3.38	3.18	2.67	2.30	1.64	1.96	1.37
Ho	0.23	0.17	0.61	0.56	0.54	0.47	0.37	0.28	0.33	0.25
Er	0.46	0.30	1.49	1.37	1.42	1.09	0.88	0.63	0.91	0.65
Tm	0.06	0.03	0.20	0.18	0.18	0.14	0.13	0.08	0.13	0.11
Yb	0.40	0.20	1.24	1.10	1.08	0.96	0.69	0.49	0.90	0.70
Lu	0.04	0.03	0.18	0.16	0.14	0.11	0.11	0.07	0.15	0.11

Column headings as in Table 1. Analyst: I.M.H.R. Antunes.

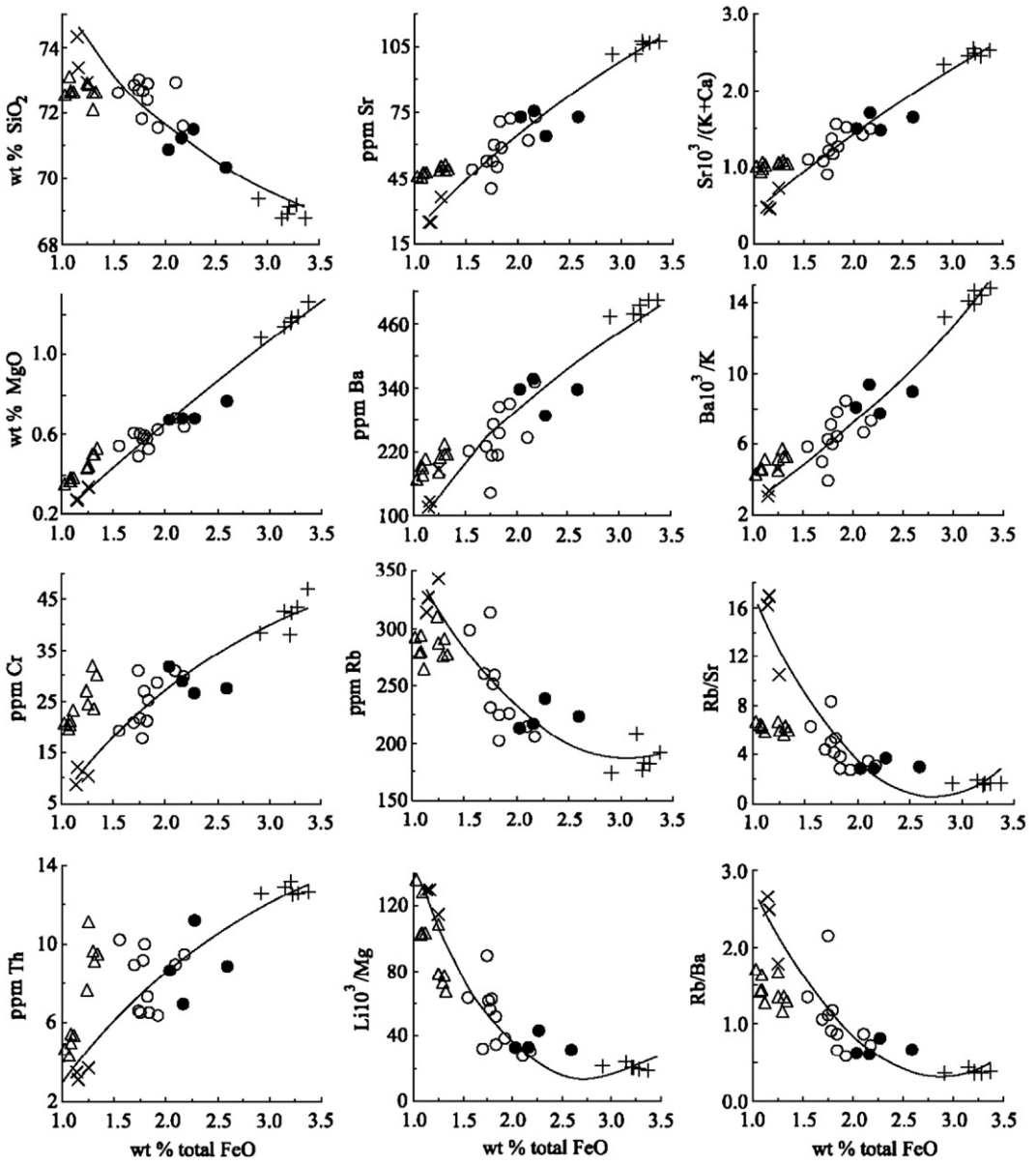

Fig. 3. Variation diagrams for selected major and trace elements and ratios of the granitic rocks from the Castelo Branco pluton. Symbols as in Fig. 2.

The slight deviation of the other two data points (fractions 6 and 7) suggests minor inheritance and some Pb loss, respectively. One analysis of monazite (fraction 9) yields a $^{207}Pb/^{235}U$ age of 310.6±1.5 Ma. Together zircon and monazite indicate formation of G2 at 310.5±1 Ma.

The third sample, representing granite G5, yields three zircon (fractions 10, 11 and 13) analyses on Concordia and one discordant (fraction 12) (Fig. 5c). A discordia line through the four points yields a lower intersect age of 309.1±0.6 Ma and an upper intersect age of about 1000 Ma. The concordant zircons alone indicate an age of 309.7±0.4 Ma, identical to the $^{207}Pb/^{235}U$ age of one of the monazite analyses (fraction 16). Two other monazite analyses (fractions 14 and 15) scatter towards higher ages; the reasons for this behaviour are not quite evident and may reflect some superimposed alteration, but a ^{230}Th disequilibrium is probable, can explain reverse discordance and may reflect a small zircon inheritance (e.g., Cocherie et al., 2005), especially in S-type granites.

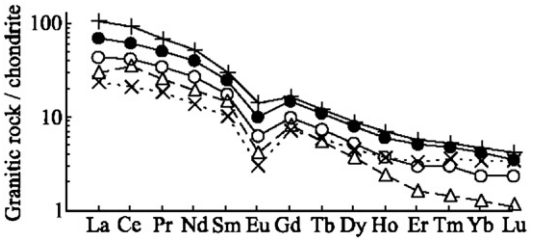

Fig. 4. Average chondrite-normalized REE abundances of the granitic rocks from the Castelo Branco pluton. Symbols as in Fig. 2.

6.2. Rb–Sr and Sm–Nd whole-rock results

The isotopic composition of Rb and Sr was measured on twelve whole-rock samples (Table 4) representing all 5 phases of the pluton. Ten samples were also analyzed for Sm and Nd (Table 4).

The initial $(^{87}Sr/^{86}Sr)_{310}$ ratios for G1, G2 and G4 are 0.7090±0.011, 0.7108±0.024 and 0.7086±0.020, respectively, and there is only one value for G3 and G5 of 0.7104 and 0.7120, respectively (Table 4). The scatter $(^{87}Sr/^{86}Sr)_{310}$ ratio suggests that the units were not in complete isotopic equilibrium at the time of formation, which is also supported by heterogeneous ε_{Nd}. This can be visualized in a plot of initial $^{87}Sr/^{86}Sr$ (310 Ma) versus ε_{Nd} (Fig. 6). The data plot within a field delimited by $\varepsilon_{Nd}=-1$ to -4 and $^{87}Sr/^{86}Sr=0.708–0.712$, which indicates derivation from crustal material with average Mesoproterozoic mantle extraction ages (Table 4). TDM values of granitic rocks are similar to the TDM data for schist metagraywacke complex from the area studied (Beetsma, 1995). The distribution of the points shows a small degree of variability within each unit (Fig. 6). The data for G1 and G4 tend to have the most negative ε_{Nd} values but variable $^{87}Sr/^{86}Sr$. Overall the data distribution requires the contribution of at least three isotopically distinct magma components (G1, G2 and G5; Fig. 6).

6.3. Oxygen isotopic data

Whole-rock oxygen-isotope ($\delta^{18}O$) values, obtained for eight representative samples of the Castelo Branco pluton, range from +12.23 to +13.65‰ (Table 5). There is a progressive increase of $\delta^{18}O$ from G2 to G3, G4 and G5. These values are also positively correlated with SiO_2, Li, Rb and negatively correlated with FeO, Sr and Ba (Fig. 7). G2, G3 and G4 define a curvilinear variation trend which is characteristic of a magmatic differentiation process. Granite G1 yields the highest value, which deviates clearly from the above trend, whereas G5 plots closer, but in average has higher $\delta^{18}O$ than the trend.

7. Mineral chemistry

7.1. Feldspars

Compositions of microcline and plagioclase are given in Table 6. Or content tends to increase and Ba content decreases from phenocryst to matrix microcline, suggesting a magmatic origin (e.g., Long and Luth, 1986). There is a decrease in anorthite content from phenocryst to matrix plagioclase (Table 6). The contents of Ba in microcline and of anorthite in plagioclase tend to decrease from G2 to G4 (Table 6 and Fig. 8). The microcline from G5 has a higher Ba content than the matrix microcline from G4 (Table 6). However, anorthite content of plagioclase in G5 is similar to lower than that of plagioclase in G4. The microcline of G2 has a higher Ba content than microcline from G1. Furthermore, anorthite content of plagioclase from G2 is higher than that of plagioclase from G1 (Table 6 and Fig. 8). Plagioclases from G3 and G4 are zoned and An content tends to decrease from core to rim (Fig. 8).

The content of phosphorus in feldspar was determined by electron microprobe in a limited number of analyses. The highest P_2O_5 values were found in feldspars from G5 (Table 6). In general, microcline has higher P_2O_5 content than coexisting plagioclase (London et al., 1990; London, 1992; Neiva, 1998). The empirical distribution coefficient $D[P]$Kf/Pl between K-feldspar and plagioclase ranges from 0.20 to 6.40. In natural feldspars close to their Or and Ab end members, like in those from the muscovite>biotite granites, G1 and G5, this coefficient should be about 1.2 for Kf–Pl pairs in equilibrium (London et al., 1999). Equilibrium was thus reached between Kf–Pl pairs in granite G5, while there is a lack of equilibrium for these pairs in granite G1. The low P content of microcline from granite G1, compared with that of albite from the same granite, identifies this microcline as formed or re-equilibrated under subsolidus conditions. However, the low $D[P]$Kf/Pl value may also reflect the continued crystallization of albite from the melt.

No clear variation was found on the P_2O_5 content from feldspar phenocryst to matrix. The P_2O_5 content of microcline is not related to its orthoclase content, and the P_2O_5 content of plagioclase does not depend on its anorthite content (Neiva, 1998), but probably depends on the phosphorus content in the crystallizing melt (Bea et al., 1994).

7.2. Micas

The average major and trace element concentrations of the analyzed biotites are given in Table 7. All are Fe^{2+}-

Table 3
U–Pb data of granitic rocks from Castelo Branco pluton, central Portugal

Granitic rocks	Mineral Characteristics[1]	Weight (μg)[2]	U (ppm)[2]	Th/U[3]	Pbc[4] (ppm)	Pbc[4] (pg)	$^{206}Pb/^{204}Pb$[5]	$^{207}Pb/^{235}U$[6]	2σ (abs.)	$^{206}Pb/^{238}U$[6]	2σ (abs.)	rho	$^{206}Pb/^{238}U$[6]	$^{207}Pb/^{235}U$[6]	$^{207}Pb/^{206}Pb$[6]	2σ (abs.)	D (%)[7]
G1																	
1	Z lp py [19]	11	206	0.10	0.06	2.7	2627	0.35722	0.00161	0.04922	0.00018	0.77	310	310	313	6.5	1.1
2	Z lp 2py [17]	26	466	0.15	0.07	3.9	10239	0.39106	0.00097	0.05298	0.00012	0.93	333	335	351	2.0	5.4
3	Z tips [24]	29	479	0.28	0.07	4.1	10929	0.37555	0.00092	0.05116	0.00011	0.92	322	324	339	2.2	5.3
4	Mz [1]	1	159	109.34	0.00	1.6	328	0.35345	0.00874	0.04931	0.00031	0.39	310	307	285	51.8	−9.2
5	Mz [1]	1	4514	4.58	4.27	6.3	2234	0.35642	0.00114	0.04931	0.00012	0.74	310	310	304	4.9	−2.1
G2																	
6	Z lp brooken [f]	61	342	0.86	0.17	12.3	5239	0.35824	0.00097	0.04926	0.00012	0.92	310	311	318	2.5	2.5
7	Z tips [30]	11	470	0.18	0.68	9.5	1695	0.35597	0.00114	0.04903	0.00012	0.72	309	309	314	5.0	1.8
8	Z lp [50]	14	424	0.88	0.05	2.7	6780	0.35725	0.00105	0.04927	0.00013	0.85	310	310	311	3.5	0.3
9	Mz [1]	1	945	26.32	0.21	2.2	1340	0.35780	0.00230	0.04951	0.00018	0.60	312	311	304	11.7	−2.7
G5																	
10	Z lp large [33]	53	585	0.13	0.03	3.7	25931	0.35678	0.00096	0.04918	0.00012	0.95	310	310	312	1.9	0.9
11	Z lp small [f]	63	478	0.14	0.08	7.1	13009	0.35680	0.00090	0.04920	0.00011	0.95	310	310	311	1.8	0.5
12	Z tips [f]	110	500	0.11	0.02	4.7	37261	0.37514	0.00097	0.05083	0.00012	0.97	320	323	351	1.5	9.2
13	Z lp brooken [49]	66	480	0.14	0.06	6.0	16319	0.35643	0.00089	0.04918	0.00011	0.95	309	310	310	1.8	0.2
14	Mz NABR [1]	2	959	24.90	1.25	4.5	1351	0.36274	0.00177	0.05023	0.00018	0.76	316	314	302	7.2	−4.8
15	Mz [13]	15	2113	14.17	0.33	6.9	14270	0.39540	0.00090	0.04976	0.00012	0.96	313	312	302	1.7	−3.8
16	Mz [7]	7	884	14.97	0.13	2.9	6606	0.35620	0.00100	0.04938	0.00011	0.85	311	309	299	3.2	−3.9

[1]Z — zircon; Mz — monazite; lp — long prismatic; py — pyramid; NABR — non-abraded (all other minerals abraded); [*N*] — number of grains in fraction (f>50 grains). All the zircons were clear and transparent. [2,4]Weight and concentrations are known to better than 10%, except for those near and below the c. 1 μg limit of resolution of the balance. [3]Th/U model ratio inferred from 208/206 ratio and age of sample. [4]Pbc is total common Pb in sample (initial+ blank). [5]Raw data corrected for fractionation. [6]Corrected for fractionation, spike, blank and initial common Pb; error calculated by propagating the main sources of uncertainty; initial common Pb corrected using Stacey and Kramers (1975) model Pb. [7]degree of discordancy. Analyst: I.M.H.R. Antunes.

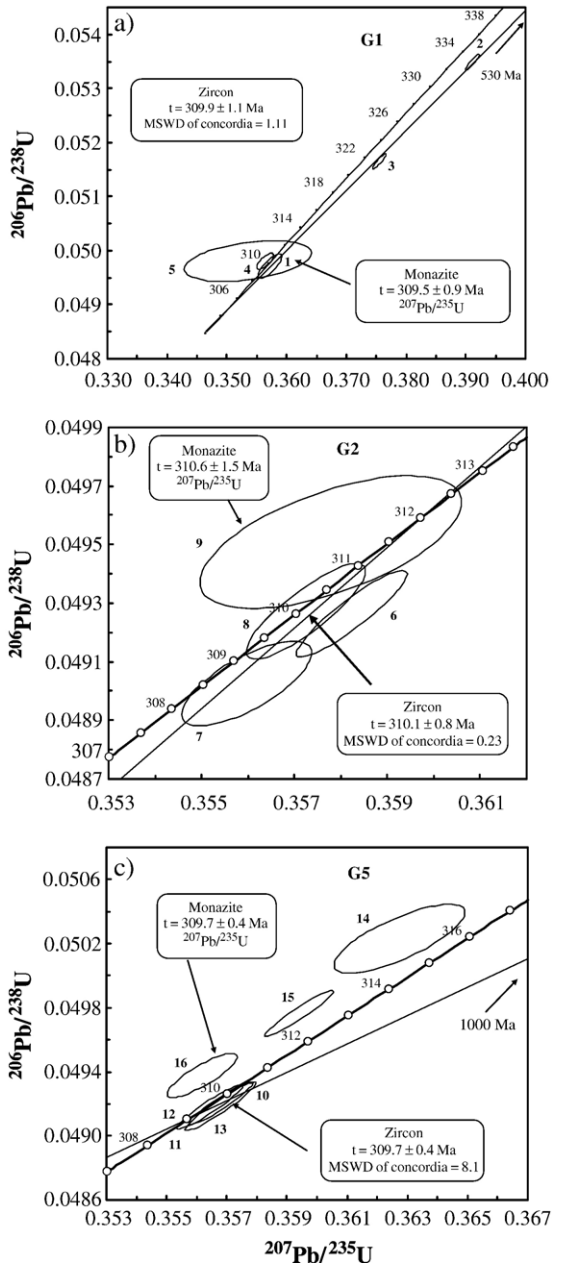

Fig. 5. Concordia diagrams displaying the U–Pb data for zircon and monazite of some granitic rocks from the Castelo Branco pluton, central Portugal. Error for ellipses are drawn at 2σ. a) Muscovite>biotite granite G1; b) Biotite>muscovite granodiorite G2; c) Muscovite>biotite granite G5.

biotite according to the nomenclature of Foster (1960) and have compositions similar to that of biotites from aluminium–potassic rock series (Nachit et al., 1985). These biotites coexist with muscovite and plot in the corresponding field in the Al_2O_3-total FeO–MgO diagram (Nockolds, 1947).

Some major and trace elements and ratios of biotite plotted against whole-rock total FeO define trends between G2 and G4 (Fig. 9a–c). In general, the data for biotite from G1 to G5 do not fit these trends.

The average major and trace element contents of the analyzed muscovite are given in Table 7. They correspond to primary muscovite according to the criteria of Miller et al. (1981) and Monier et al. (1984).

Variation diagrams for trace elements and ratios of muscovite versus whole-rock total FeO show a trend from G2 to G4 (Fig. 9d–f) except for the data of muscovite from granites G1 and G5 that tend to deviate from the trend.

$D_{Ti}^{Bt/Ms}$ and $D_{F}^{Bt/Ms}$ of 6.11–13.09 and 2.14–9.93, respectively in G3 and G4, are higher than those of coexisting micas in peraluminous experimental systems (Icenhower and London, 1995). F_{Ap}/F_{Bt} and F_{Ap}/F_{Ms} in G3 and G4 are 9.05, 6.58 and 33.48, 35.19, respectively, showing a systematic partitioning of F between apatite and the micas, which suggests equilibrium conditions (Clarke et al., 2005). Therefore, biotite, muscovite and apatite are primary.

7.3. Andalusite and sillimanite

Andalusite and sillimanite occur as accessory minerals in peraluminous granodiorite G3 and granite G4, but sillimanite also occurs in G2. These granitic rocks have average A/CNK ratios ranging from 1.14 to 1.16. Sillimanite was found included in andalusite. Euhedral andalusite grains have similar dimensions to those of other magmatic minerals. Andalusite is relatively pure, containing up to 0.47 wt.% FeO. The sillimanite needles could not be analyzed.

The coexisting biotite has Al^{IV} ranging between 1.325 and 1.345 (on the basis of 11 atoms of oxygen), suggesting that the biotite is in equilibrium with some Al-rich phase, such as andalusite, probably under conditions of restricted temperature and pressure. Consequently biotite and andalusite are magmatic (Clarke et al., 2005). Andalusite also coexists with magmatic muscovite and apatite. Both andalusite and sillimanite are early minerals in the crystallization sequence. The studied andalusite corresponds to the cotectic type 2c (water-undersaturated, T↓) of Clarke et al. (2005).

7.4. Cordierite

Cordierite was found in granodiorite G3 and granite G4. Chemical analyses are given in Table 8. The euhedral crystals do not contain inclusions and have

Table 4
Isotopic whole-rock data of granitic rocks from the Castelo Branco pluton, central Portugal

Granitic rocks	Rb (ppm)	Sr (ppm)	$^{87}Rb/^{86}Sr$	$^{87}Sr/^{86}Sr$	Error% (2 σ)	$(^{87}Sr/^{86}Sr)_{310}$	Sm (ppm)	Nd (ppm)	$^{147}Sm/^{144}Nd$	$^{143}Nd/^{144}Nd$	% Error	$(^{43}Nd/^{44}Nd)_{310}$	$^{\varepsilon}Nd_{310}$	T_{DM310}
G1														
GCL7	273	49	17.894	0.7871	0.003	0.7082	2.989	13.106	0.1379	0.51233	0.002	0.51205	−3.6	1.52
PAL7	288	43	22.286	0.8081	0.003	0.7098	2.526	10.23	0.1493	0.512336	0.002	0.51203	−4.0	1.75
G2														
GIN	192	113	4.534	0.7312	0.002	0.7112	7.221	38.217	0.1142	0.512356	0.0019	0.51212	−2.2	1.15
GIN2	207	107	4.924	0.7343	0.002	0.7128	6.587	35.423	0.1124	0.512405	0.002	0.51218	−1.2	1.06
GIN4	117	113	4.833	0.7301	0.003	0.7085	7.015	38.802	0.1093	0.512370	0.002	0.51215	−1.8	1.08
G3														
REPA	212	74	8.234	0.7467	0.002	0.7104	4.637	22.7	0.1235	0.512448	0.003	0.51220	−0.8	1.11
G4														
GM	294	47	20.481	0.7981	0.002	0.7078	3.246	15.277	0.1285	0.512319	0.002	0.51206	−3.5	1.38
GC	256	48	15.874	0.7784	0.002	0.7084	–	–	–	–	–	–	–	–
G13	230	52	14.102	0.7706	0.002	0.7084	–	–	–	–	–	–	–	–
GVR	214	62	10.141	0.7551	0.004	0.7104	4.133	19.079	0.1310	0.512407	0.002	0.51214	−1.9	1.27
NAC	309	37	28.181	0.8326	0.020	0.7082	3.183	14.578	0.1320	0.512349	0.002	0.51208	−3.1	1.39
G3														
LARDO	337	332	25.111	0.8462	0.002	0.7120	2.770	11.577	0.1446	0.512380	0.002	0.51209	−3.0	1.56

– Not determined. TDM age was calculated based on values of De Paolo (1981).

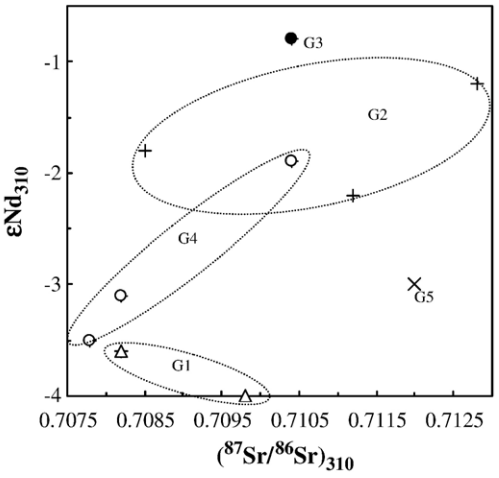

Fig. 6. Diagram of $(^{87}Sr/^{86}Sr)_{310}$ versus εNd_{310} of granitic rocks from Castelo Branco. Symbols as in Fig. 2.

Na_2O >0.5 wt.%, suggesting a magmatic origin (e.g., Bouloton, 1992; Villaseca and Barbero, 1994; Williamson et al., 1997). According to Clarke (1995), it corresponds to the type 2c cotectic magmatic cordierite. A similar cordierite occurs in the Alpine cordierite-bearing granitoids of northern Algeria (Fourcade et al., 2001). It also corresponds to magmatic cordierite in the Na+K versus Mg/(Mg+Fe+Mn) diagram of Pereira and Bea (1994).

The cordierite from the Castelo Branco pluton has higher $Al^{IV}+Al^{VI}$, Ca, Na, K and lower Mg and Mg/(Mg+Fe) values than metamorphic cordierite from central Portugal (Pereira et al., 1993; Silva and Neiva, 1999/2000; Pinto, 2001). The magmatic cordierite from the Castelo Branco pluton is also richer in Ca, Na and poorer in Mg and Mg/(Mg+Fe) than magmatic cordierite of the biotite granite from Tondela-Oliveira do Hospital (Pereira et al., 1993) and the Carregal do Sal-Nelas-Lagares da Beira area, central Portugal (Silva and Neiva, 1999/2000).

There is an increase in Si, Al^{VI}, Mn, Na and decrease in Al^{IV}, Fe, Mg and Ca from the cordierite of biotite>muscovite granodiorite G3 to the cordierite of biotite=muscovite granite G4 (Table 8).

7.5. Ilmenite

Ilmenite occurs in all granitic rocks from the Castelo Branco pluton. A negative correlation between Ti and Fe+Mn of ilmenite was found. MnO ranges from 1.81 to 4.87 wt.%. Mn and Mn/(Mn+Fe) increase and Fe decreases from the ilmenite of biotite>muscovite granodiorite G2 to the ilmenite of biotite=muscovite granite G4.

8. Petrogenesis

The variation diagrams for major and trace elements, trace/major element ratios of peraluminous granitic rocks G2 to G5 (Fig. 3) and the decrease in Ca of plagioclase from G2 to G5 (Table 6 and Fig. 8) support the occurrence of magma differentiation.

Table 5
$\delta^{18}O$ values in ‰ and some major and trace element contents of selected samples of whole-rock granitic rocks from Castelo Branco pluton, central Portugal

Granitic rocks	$\delta^{18}O$ (‰)	SiO_2 (wt.%)	Total FeO (wt.%)	Li (ppm)	Sr (ppm)	Ba (ppm)	Rb (ppm)
G1							
GCL7	13.42	72.09	1.30	201	49	234	273
GEB2	13.65	73.10	1.07	199	42	194	275
G2							
GIN	12.23	68.80	3.37	141	113	502	192
INFX2	12.31	69.37	2.91	133	106	473	174
G3							
PC	12.50	70.36	2.59	139	74	337	222
G4							
NAC	12.75	72.99	1.74	172	37	144	309
G5							
SO2	13.14	73.35	1.16	176	19	129	321
LC1	12.68	74.27	1.14	175	20	116	309

Table 6
Compositions of feldspars of the granitic rocks from the Castelo Branco pluton, central Portugal

Granitic rocks	G1	G2	G3	G4	G5
Or content of K-feldspar					
Phenocrysts	–	91–95	92–96	95	–
Matrix	94	94	96	92–97	92–97
wt.% BaO of K-feldspar					
Phenocrysts	–	0.31	0.24	0.24	–
Matrix	0.12	0.25	0.09	0.09	0.17
An content of plagioclase					
Phenocrysts	–	–	10–23	3–17	–
Matrix	1–7	4–23	01–19	0–14	1–8
wt.% P_2O_5					
K-feldspar	0.03	0.29	0.11	0.32	0.60
Plagioclase	0.15	0.06	0.08	0.05	0.43
D[*P*]Kf/Pl	0.20	4.83	1.38	6.40	1.40

Column headings as in Table 1. *D*[*P*]Kf/Pl — empirical distribution coefficient. Analyst: I.M.H.R. Antunes.

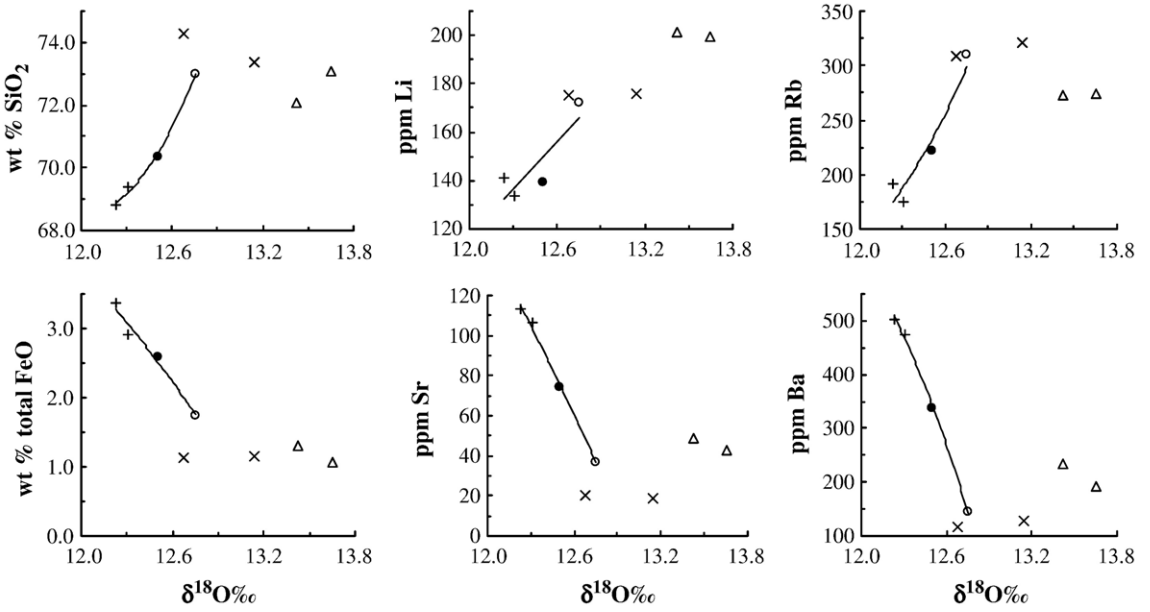

Fig. 7. Selected variation diagrams of $\delta^{18}O$ of the granitic rocks from the Castelo Branco pluton. Symbols as in Fig. 2.

The granitic rocks G2, G3 and G4 show gradational field contacts between them (Fig. 1), their rare earth element patterns are subparallel (Fig. 4), their biotite and muscovite define differentiation trends from trace elements (Fig. 9), suggesting that they define a series. The positive correlations between $\delta^{18}O$ and SiO_2, Li and Rb and the negative correlations between $\delta^{18}O$ and total FeO, Sr and Ba for the granitic rocks G2, G3 and G4 with $\delta^{18}O$ increasing from 12.27 in granodiorite G2 to 12.75‰ in granite G4 (Table 5 and Fig. 7) can be attributed to a fractional crystallization process, which can present a variation of $\delta^{18}O$ from 1 to 1.2‰ (e.g., White, 2003). There was no oxygen-isotope exchange at subsolidus temperature between feldspar and quartz, because it would decrease the $\delta^{18}O$ values of these granitic rocks (Blattner et al., 2002). The isotopic Sr and Nd values show some differences in G2, G3 and G4 and even within individual granite type (Fig. 6), but they are not very large. G2 is a crustal-derived magma highly susceptible to be isotopically heterogeneous (e.g., Brown and Pressley, 1999). There are many geochemical and isotopic correlations that support a link between G2, G3 and G4 by fractional crystallization.

The relationship between the peripherical unit G5 and G4 is more ambiguous. The geochemical parameters of G5 (for example the higher Ba content of microcline in G5

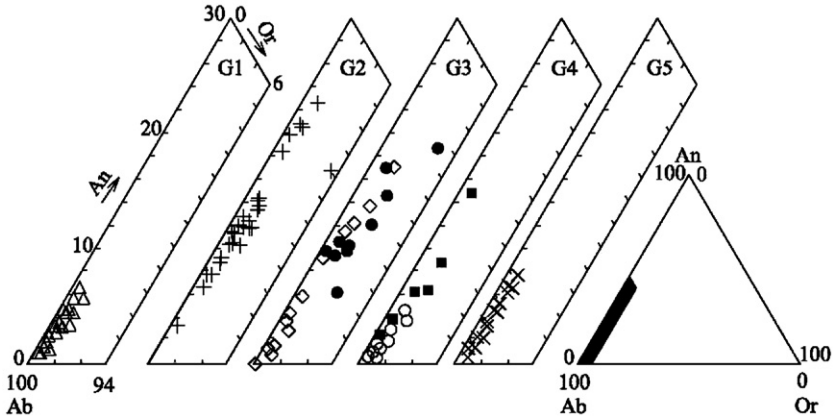

Fig. 8. Plot of plagioclase compositions from the granitic rocks of the Castelo Branco pluton. Symbols as in Fig. 2; close symbols — core and open symbols — rim.

Table 7
Chemical analyses (EPMA) in wt.% and trace elements (ICP-MS) in ppm of biotites and muscovites of granitic rocks from the Castelo Branco pluton, central Portugal

	G1		G2		G3		G4		G5	
	bt	mv	bt	mv	bt	mv	bt	mv	bt	mv
SiO_2	34.80	46.39	35.17	46.20	34.39	45.65	34.82	46.69	34.44	47.09
TiO_2	2.84	0.61	3.00	0.68	2.53	0.26	2.88	0.41	2.26	0.33
Al_2O_3	19.17	35.57	18.75	35.43	19.11	35.30	19.57	35.77	19.12	34.17
Fe_2O_3	1.57	0.11	0.37	0.04	1.11	0.10	0.89	0.11	2.73	0.14
FeO	20.91	0.98	20.27	0.90	21.64	0.86	21.80	1.06	22.57	1.25
MnO	0.22	0.01	0.20	0.01	0.24	0.01	0.25	0.02	0.30	0.03
MgO	5.22	0.72	7.19	0.65	6.30	0.59	5.21	0.66	3.90	0.73
CaO	0.01	0.01	0.02	0.01	0.02	0.01	0.01	0.01	0.03	0.01
Na_2O	0.05	0.71	0.12	0.69	0.10	0.76	0.11	0.79	0.06	0.55
K_2O	9.03	10.31	9.35	10.51	9.16	10.33	9.21	10.24	9.30	10.34
Cl	0.01	–	0.03	–	0.02	0.01	0.02	–	–	–
F	0.79	0.23	0.63	0.12	0.75	0.23	0.86	0.17	–	0.01
	94.62	95.66	95.10	95.24	95.37	94.11	95.63	95.93	94.70	94.65
O≡Cl	–	–	0.01	–	–	–	0.01	–	–	–
O≡F	0.33	0.10	0.26	0.05	0.32	0.10	0.36	0.07	–	–
Total	94.29	95.55	94.83	95.19	95.05	94.01	95.27	95.86	94.70	94.65
Ga	52	95	47	72	59	81	7	82	69	111
Cr	69	14	189	25	122	20	124	17	57	16
V	113	40	269	84	248	65	218	50	94	36
Nb	118	33	89	12	118	21	132	30	156	52
Zn	1085	82	334	36	570	44	686	58	1335	102
Sn	42	76	23	50	35	68	59	101	64	88
W	*	20	*	12	*	17	*	33	*	12
Li	2855	607	969	120	1250	200	2040	426	2370	659
Ni	30	*	60	*	46	5	47	*	39	*
Co	13	9	29	5	25	*	*	*	14	*
Zr	87	25	133	18	87	25	96	20	93	28
Cu	24	8	26	9	18	11	26	13	11	6
Sc	12	19	38	38	39	31	31	18	11	27
Y	7	*	14	*	8	*	12	*	14	*
Ba	184	220	1029	485	327	356	216	244	94	116
Rb	1343	816	786	446	1120	557	1230	776	1700	1035
Cs	248	122	100	28	150	34	170	74	221	73
Ta	24	9	14	*	21	*	27	16	23	*
Pb	7	*	8	*	9	*	14	*	9	*
Th	19	*	18	*	15	*	11	*	13	*

Column headings as in Table 1. bt — biotites; mv — muscovites. – Not detected. * — below the limit of sensitivity. Analyst: I.M.H.R. Antunes.

than G4; the REE pattern of G5 crossing that of G4 at Ho in Fig. 4; variation diagrams for biotite and muscovite shown in Fig. 9) also tend to fit poorly those of the G2–G4 series indicating slightly different sources.

The field contact between muscovite>biotite granite G1 cropping out in the core of the pluton and biotite>muscovite granodiorite G2 is sharp. G1 does not fit the differentiation trends for whole-rocks (Figs. 3 and 7) and its REE pattern crosses that of G5 at Gd in Fig. 4. There is some resemblance between G1 and G5 in terms of mineralogy, as they are granites containing more muscovite than biotite (Table 1), have a similar anorthite content of plagioclase (Table 6), plot close in the variation diagrams for biotite and muscovite and do not fit the fractionation trends for micas from G2, G3 and G4 (Fig. 9). The mean initial $(^{87}Sr/^{86}Sr)_{310}$ ratios for G1 and G2 are 0.7090 ± 0.011 and 0.7108 ± 0.024, respectively, and there is one value for G5 of 0.7120 ± 0.0002 (Table 4 and Fig. 6), suggesting that they correspond to three distinct magma pulses. This is confirmed by contrasting mean εNd_{310} values of −3.8, −1.7 and −3.0, respectively, along with distinct $\delta^{18}O$ mean values (G1 — 13.54; G2 — 12.17; G5 — 12.91‰). These granitic rocks are peraluminous with A/CNK ratio ≥1.1, contain normative corundum ≥2.8, have LREE-enriched chondrite-normalized patterns, a negative Eu anomaly, initial $^{87}Sr/^{86}Sr \geq 0.7090$ and $\delta^{18}O \geq 12.27$‰. These features are compatible with S-type granites (Chappell and White, 1992). The chemical differences between G1,

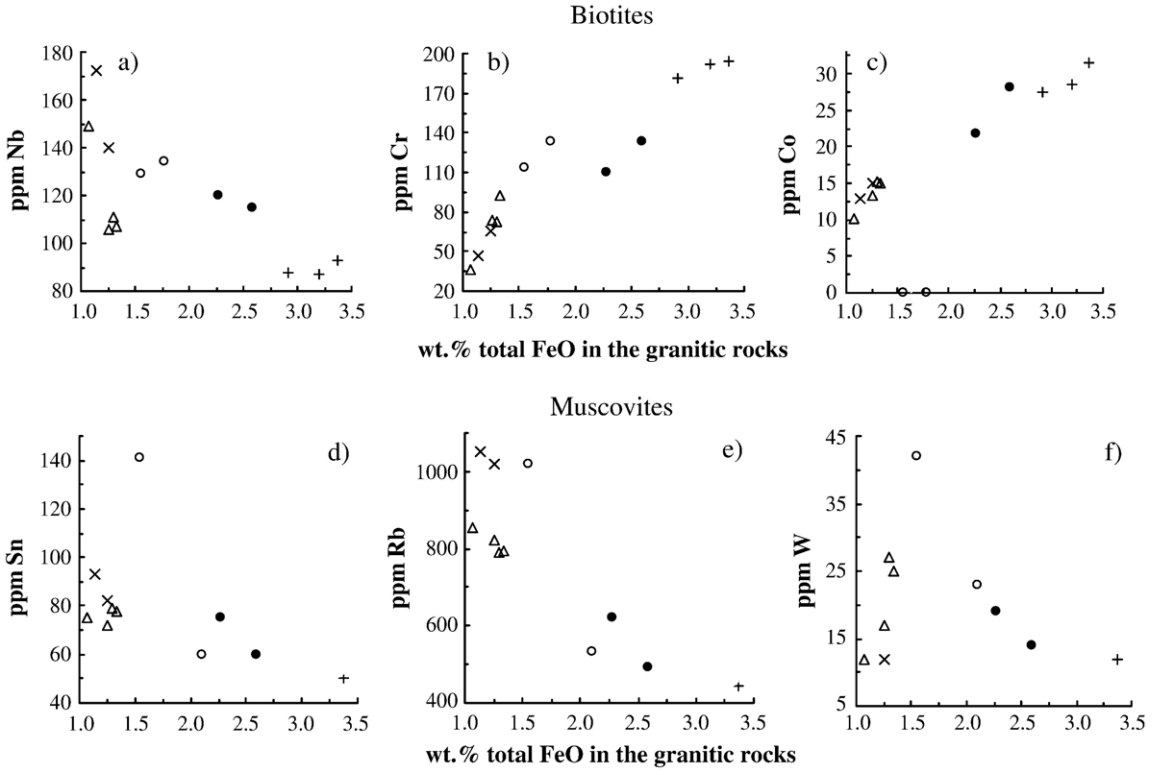

Fig. 9. Variation diagrams of some trace elements of biotites and muscovites from granitic rocks of the Castelo Branco pluton. Symbols as in Fig. 2.

G2 and G5 are attributed to the heterogeneity of the metasedimentary source and reflect rapid rates of extraction, ascent and emplacement of individual batches (Brown and Pressley, 1999). These granitic rocks were emplaced in the Cambrian schist–metagraywacke complex, consisting of phyllite with intercalations of metagraywacke and marble. Inherited zircons cores point to an Early Paleozoic component in the source (Cambrian upper intercept age; Fig. 5a) together with Precambrian detritus (ca. 1 Ga upper intercept age; Fig. 5c). It is possible that the source was similar in composition to this heterogeneous country rock.

An equilibrium batch melting model evolves a similar or close melt composition and similar REE concentrations to the source rock (Dahlquist et al., 2005), in which the melt reacts continually and in situ re-equilibrates. In a batch partial melting series, the least silicic samples represent a melt derived from a higher degree of partial melting than the most silicic samples as the melt has higher contents of Ti, Fe, Mg, Ca, Ba, Zr and Ce with increase in temperature (Holtz and Barbey, 1991; Bogaerts et al., 2003). The granodiorite G2 has major, trace and rare earth element contents which suggest that it may be derived from a higher degree of partial melting than muscovite-dominant granites G1 and G5 (Table 1).

Furthermore, G1 has higher Mg, Cr, Sr, Ba, Th and LREE contents and lower Rb content than G5 indicating that it may represent a higher degree of partial melting than G5. However, the differences in $(^{87}Sr/^{86}Sr)_{310}$, εNd_{310} and $\delta^{18}O$ of G1, G2 and G5 (Tables 4 and 5) are too large to be explained by batch melting and consequently they will be mainly due to heterogeneity of the metasedimentary source.

Major and trace element contents of granodiorites G2, G3 and granites G4 and G5 were used to test fractional

Table 8
Electron microprobe chemical analyses in wt.% and cations based on 18 atoms of oxygen of cordierites of granitic rocks from the Castelo Branco pluton, central Portugal

	G3	G4		G3	G4
SiO_2	47.89	48.67	Si	5.033	5.074
TiO_2	–	–	Al^{IV}	0.967	0.926
Al_2O_3	32.87	33.16	Al^{VI}	3.105	3.149
FeO	11.08	10.35	Ti	–	–
MnO	0.02	0.28	Fe^{2+}	0.974	0.903
MgO	4.13	4.08	Mg	0.647	0.634
CaO	0.38	0.11	Mn	0.002	0.024
Na_2O	1.30	1.56	Ca	0.043	0.012
K_2O	0.40	0.15	Na	0.265	0.315
Total	98.07	98.36	K	0.053	0.020
			Mg*	0.40	0.41

– Not detected. Mg* = Mg/(Mg + Fe + Mn). Analyst: I.M.H.R Antunes.

crystallization. The average of the two least silicic samples of granodiorite G2 was selected as the starting magma, while the most silicic sample of G2, the average composition of G3, the mean of the seven most silicic samples of G4 and the average composition of G5 were selected as residual liquids. The least-squares regression method was applied to model major elements, taking pure anorthite, albite, potash feldspar and quartz, and the compositions of biotite, muscovite and ilmenite, determined by electron microprobe, in the least silicic sample of granodiorite G2. The sum of the squares of the residuals (ΣR^2) should be <1.0 and is ≤ 0.24, except for G5, showing 0.87 (Table 9). The anorthite content of the fractionating plagioclase is close to the highest value found in the plagioclase of granodiorite G2 (Tables 6 and 9). The percentage of quartz increases and that of plagioclase decreases in the cumulate versus the decrease in the weight fraction of melt remaining during fractional crystallization (Fig. 10). The muscovite>biotite granite G5 plots outside the trends, showing that it does not belong to the sequence.

The Rayleigh fractionation equation, the modal compositions of cumulate and weight fraction of melt remaining during fractional crystallization based on calculations involving major elements and the distribution coefficients of Peccerillo et al. (1994) were used for modelling Sr, Ba and Rb, which are the most informative trace elements for evaluating the fractionation of granitic rocks. Sr decreases and Rb, Rb/Sr and Rb/Ba increase versus a decrease in the residual melt fraction during fractional crystallization (Fig. 10) from biotite>muscovite granodiorite G2 to biotite–muscovite granite G4. The muscovite>biotite granite G5 does not fit the trends. The calculated Sr, Ba and Rb values for the most silicic sample of G2 are similar to the analytical data (Table 9 and Fig. 11). The calculated Sr and Ba values for G3 and G4 are higher than the analytical data, while the calculated Rb, Rb/Ba and Rb/Sr ratios are lower than the analytical data (Fig. 11), because the distribution coefficients have large errors and magmatic fluids may have controlled the behaviour of LIL elements in the most evolved granitic rocks. However, the differences between calculated and

Table 9
Results of the fractional crystallization modelling of granitoids from Castelo Branco pluton, central Portugal

	Determined starting granodiorite magma	Calculated composition of starting magma for			
	G2	G2	G3	G4	G5
		Calc.	Calc.	Calc.	Calc.
SiO_2	69.29	69.30	69.30	69.30	69.40
TiO_2	0.56	0.50	0.50	0.50	0.60
Al_2O_3	15.84	15.80	15.80	15.80	16.00
Fe_2O_3t	3.65	3.24	2.52	1.94	1.31
MgO	1.16	1.20	1.10	1.10	1.10
CaO	1.46	1.50	1.50	1.50	1.40
Na_2O	3.96	4.00	4.00	4.00	3.90
K_2O	4.08	4.10	4.10	4.10	4.00
FR		0.885±0.017	0.735±0.008	0.697±0.012	0.622±0.051
$\sum R^2$		0.05	0.08	0.24	0.87
Modal composition of cumulate					
Quartz		21.1±4.4	23.0±2.3	24.7±4.0	17.7±3.4
Plagioclase		52.6±7.0	49.0±4.1	44.2±0.9	50.8±5.8
Biotite		26.3±3.5	28.0±1.5	30.7±0.7	30.7±2.1
Ilmenite		–	–	0.4±0.0	0.8±0.5
%An of plagioclase		27.0±1.4	30.0±1.0	28.4±8.1	27.0±1.3

Composition of residual melts

		G2		G3		G4		G5	
ppm	Det.	Det.	Calc.	Det.	Calc.	Det.	Calc.	Det.	Calc.
Sr	110	106	96	72	85	52	82	23	66
Ba	490	473	472	331	438	297	373	144	337
Rb	170	174	171	224	170	253	178	322	150

G2, G3, G4 and G5 as in Table 1. FR — weight fraction of melt remaining during fractional crystallization; ΣR^2 — sum of the squares of the residuals; — not fractionated. Det. — determined; Calc. — calculated.

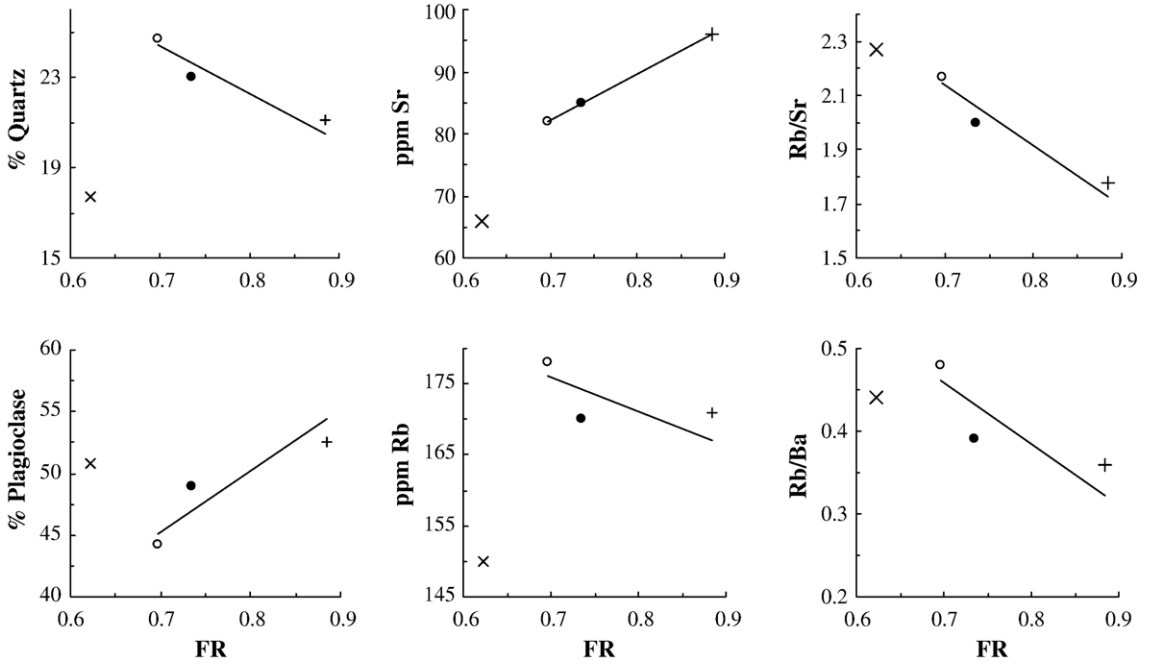

Fig. 10. Plot of modal quartz and plagioclase of cumulate and of calculated trace element contents and ratios in granitic rocks from the Castelo Branco pluton versus weight fraction of melt remaining during fractional crystallization. Symbols as in Fig. 2. FR — weight fraction of melt remaining during fractional crystallization.

analyzed trace element contents for G3 and G4 are much smaller than those for G5, as G5 does not belong to the series G2–G4 (Fig. 10).

Modelling of REE was also attempted using the calculated modal compositions of cumulate and weight fraction of melt remaining during fractional crystallization (Table 9) and partitioning REE coefficients for plagioclase (Demaiffe and Hertogen, 1981) and ilmenite (Nakamura et al., 1986). LREE show an overall increase relatively to MREE and HREE due to plagioclase fractionation, which is also responsible for Eu fractionation (Vander Auwera et al., 1998). However the calculated REE patterns show an increase in LREE, MREE and HREE from G2 to G4 which is opposite to the behaviour of REE (Fig. 4) due to the fact that most REE of granitic rocks are concentrated in accessory minerals. The decrease in LREE from granodiorite G2 to granite G4 (Fig. 4) can be attributed to fractionation of monazite, while the decrease in MREE can be explained by fractionation of apatite and zircon as the decrease in HREE is due to fractionation of zircon (Mittlefehldt and Miller, 1983; Yurimoto et al., 1990), as evidenced by the decrease in Zr from G2 to G4 (Table 1).

The granodiorite G3 and granite G4 contain primary andalusite, sillimanite and cordierite, which were formed during fractional crystallization of granodiorite G2 magma. Andalusite and sillimanite may have been formed as the result of plagioclase fractionation from the peraluminous granodiorite G2 magma, when Al_2SiO_5 magma saturation was reached (Frank et al., 1998), while cordierite is probably a consequence of biotite fractionation as represented by the reaction biotite + aluminosilicate + quartz = cordierite + K-feldspar + melt (Clarke, 1995).

As the muscovite>biotite granite G5 fits the fractionation trends defined by the granitic rocks G2, G3 and G4 (Fig. 3), but is not derived from granodiorite G2 magma by fractional crystallization (Fig. 10) and has a higher initial $(^{87}Sr/^{86}Sr)_{310}$ ratio compared with that of G2, G3 and G4 (Table 4), it is thought that it may have resulted from an AFC process (assimilation of metasediments contemporaneously with the fractional crystallization). The AFC model was tested using the equation proposed by De Paolo (1981), the Rb, Sr and initial $^{87}Sr/^{86}Sr$ ratio of the least silicic sample of granodiorite G2 and assuming that the assimilated country rock had 180 ppm Rb, 54 ppm Sr and initial $^{87}Sr/^{86}Sr = 0.73$ (at 310 Ma), which are the average values for the Cambrian metapelitic-metagraywacke rocks, also similar to the composition to those of the studied area (Reavy et al., 1991). The model shows that the granite G5 could not have been formed by this process and therefore it corresponds to a contemporaneous but distinct pulse of granite magma, enriched on $^{87}Sr/^{86}Sr$ initial ratio (Table 4) and with distinct εNd_{310} and $\delta^{18}O$ values (Tables 4 and 5).

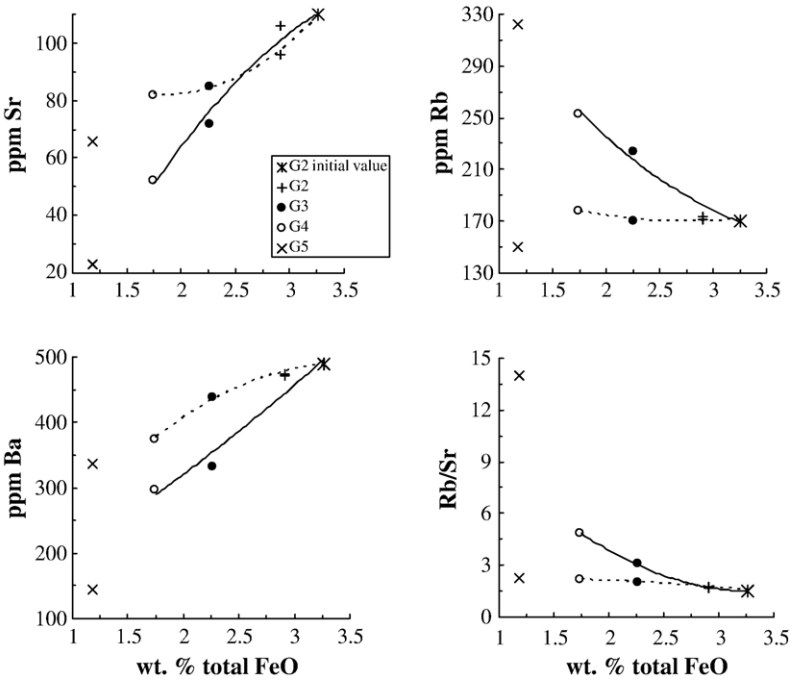

Fig. 11. Variation diagrams of Sr, Ba, Rb contents and Rb/Sr ratio values of granitic rocks from Castelo Branco pluton compared to results from modelling studies. Symbols as in Fig. 2; * — granodiorite G2, initial concentration; solid line for analytical data and broken line for calculated values.

The muscovite>biotite granite G1 in the pluton's core was the first to be emplaced, as it represents a distinct pulse of granite magma and is encircled by biotite>muscovite granodiorite G2 which represents the starting magma that by in situ fractional crystallization originated the other biotite>muscovite granodiorite G3 and biotite=muscovite granite G4 outwards, because granite G1 was inwards. The early crystallized minerals separated from melt mainly by gravity, but fluids played also a role for G3 and G4, as a result of late stage fractional crystallization (Winter, 2001). Muscovite>biotite granite G5 corresponds to another distinct pulse of granite magma which partially encircles G4, as it forms some external parts of the pluton, and was the last to be emplaced. The emplacement process was very rapid lasting less than two Ma uncertainty. Therefore, the combined geological, geochemical and isotopic data set indicates that the Castelo Branco pluton consists of three distinct magmatic pulses intruded successively and the fractional crystallization of the granodiorite magma G2 to form a reversely zoned pluton younging outwards. The reverse zoning of the pluton is uncommon (e.g., Allen, 1992; Barbey et al., 2001), especially as an S-type granite.

9. Conclusions

1) The whole-rock $\delta^{18}O$ defines a trend from the biotite>muscovite granodiorite G2 to the biotite=muscovite granite G4, but the muscovite>biotite granites G1 and G5 do not fit the trend.

2) Biotites and muscovites of granitic rocks G2, G3 and G4 show trends of fractionation for major and trace elements and ratios from granodiorite G2 to granite G4. The biotites and muscovites of granites G1 and G5 do not fit the general trends.

3) The granodiorite G3 and granite G4 are the products of in situ fractional crystallization of granodiorite magma G2 controlled by separation of plagioclase, quartz, biotite and ilmenite, which took place outwards in maximum two million years.

4) The muscovite>biotite granites G1 and G5 and biotite>muscovite granodiorite G2 have distinct initial $^{87}Sr/^{86}Sr$ ratios and εNd_T values and the geochemistry of their micas and $\delta^{18}O$ values indicate that they arose from partial melting of the heterogeneous pelitic country rock. The mean U–Pb age obtained for zircon and monazite from each granitic rock G1, G2 and G5 is 310 ± 1 Ma, showing that they are contemporaneous.

5) The Castelo Branco pluton shows an uncommon zoning resulting from a pulse of granite magma G1 in the pluton's core, followed by a pulse of granodiorite magma G2 surrounding G1 and differentiating to originate granodiorite G3 and granite G4 outwards. Another distinct pulse of granite magma originated G5 outwards.

Acknowledgments

This paper corresponds to a synthesis of a part of the PhD thesis of I.M.H.R. Antunes. Thanks are due to Prof. R. Nesbitt and Prof. I.W. Croudace for the XRF facilities provided at the Southampton Oceanography Centre, U.K.; Prof. B.J. Wood of the EUGF-Bristol research facility, for the use the electron microprobe; Prof. A.C. Fernandèz for the facilities at Laboratório de Geologia e Geocronologia of the University of Oviedo, Spain; Prof. F. Bea and Prof. P. Montero for the Rb–Sr and Sm–Nd isotopic data obtained at the Centro de Instrumentación Científica of the University of Granada, Spain; Prof. F.J. Longstaffe for the oxygen-isotope analyses obtained at the Department of Earth Sciences, University of Western Ontario, Canada. Funding was provided to I.M.H.R. Antunes by the SFRH/BD/2885/2000 grant from Fundação para a Ciência e a Tecnologia, Portugal, another grant from the SOCFAC — Southampton Oceanography Centre Facilities, Access and Co-Operation at the Southampton Oceanography Centre, U.K., and a third grant by the EU Geochemical Facilities at the University of Bristol, U.K. This research was carried out under the Geoscience Centre programme, University of Coimbra, Portugal. This paper benefited from the very helpful reviews by N. Eby (Editor), F. Bussy and an anonymous referee.

References

Allen , C.M., 1992. A nested diapir model for the reversely zoned Turtle Pluton, southeastern California. Trans. R. Soc. Edinb. Earth Sci. 83, 179–190.

Almeida, M.A., Martins, H.C., Noronha, F., 2002. Hercynian acid magmatism and related mineralizations in northern Portugal. Gondwana Res. 5, 423–434.

Antunes, I.M.H.R., 2006. Mineralogia, Geoquímica e Petrologia de rochas granitóides da área de Castelo Branco-Idanha-a-Nova. Unpublished Ph D. thesis. University of Coimbra, Portugal, 453 pp.

Azevedo, M.R., Nolan, J., 1998. Hercynian late-post-tectonic granitic rocks from the Fornos de Algodres area (northern central Portugal). Lithos 44, 1–20.

Barbey, P., Nachit, H., Pons, J., 2001. Magma-host interactions during differentiation and emplacement of a shallow-level, zoned granitic pluton (Tarçovate pluton, Morocco): implications for magma emplacement. Lithos 58, 125–143.

Bea, F., Pereira, M.D., Corretgé, L.G., Fershtater, G.B., 1994. Differentiation of strongly peraluminous posphosphorus granites. The Pedrobernado pluton, central Spain. Geochim. Cosmochim. Acta 58, 2609–2628.

Beetsma, J.J., 1995. The late Proterozoic/Paleozoic and Hercynian crustal evolution of the Iberian Massif, N Portugal. Unpublished Ph D. thesis. Vrije Universiteit Amsterdam, 223 pp.

Blattner, P., Abart, R., Adams, C.J., Faure, K., Hui, L., 2002. Oxygen isotope trends and anomalies in granitoids of the Tibetan plateau. J. Asian Earth Sci. 21–3, 241–250.

Bogaerts, M., Scaillet, B., Liégeois, J.P., Vander Auwera, J., 2003. Petrology and geochemistry of the Lyngdal granodiorite (Southern Norway) and role of fractional crystallisation in the genesis of Proterozoic ferro-potassic A-type granites. Precambrian Res. 124, 149–184.

Bouloton, J., 1992. Mise en évidence de cordiérite héritée des terrains traversés dans le pluton granitique des Oulad Ouaslam (Jebilet, Maroc). Can. J. Earth Sci. 29, 658–668.

Brown, M., Pressley, R.A., 1999. Crustal melting in nature: prosecuting source processes. Phys. Chem. Earth, Part A Solid Earth Geod. 24 (3), 305–316.

Chappell, B.W., White, A.J.R., 1992. I- and S-type granites in the Lachlan Fold Belt. Trans. R. Soc. Edinb. Earth Sci. 83, 1–26.

Clarke, D.B., 1995. Cordierite in felsic igneous rocks: a synthesis. Mineral. Mag. 59, 311–325.

Clarke, D.B., Dorais, M., Barbarin, B., Barker, D., Cesare, B., Clarke, G., El Baghdadi, M., Erdmann, S., Förster, H.-J., Gaeta, M., Gottesmann, B., Jamieson, R.A., Kontak, D.J., Koller, F., Gomes, C.L., London, D., Morgan VI, G.B., Neves, L.J.P.F., Pattison, D.R.M., Pereira, A.J.S.C., Pichavant, M., Rapela, C.W., Renno, A.D., Richards, S., Roberts, M., Rottura, A., Saavedra, J., Sial, A.N., Toselli, A.J., Ugidos, J.M., Uher, P., Villaseca, C., Visona, D., Whitney, D.L., Williamson, B., Woodard, H.H., 2005. Occurrence and origin of andalusite in peraluminous felsic igneous rocks. J. Petrol. 46, 441–472.

Cocherie, A., Mezeme, E.B., Legendre, O., Fanning, C.M., Faure, M., Rossi, P., 2005. Electron-microprobe dating as a tool for determining the closure of Th–U–Pb systems in migmatitic monazites. Am. Mineral. 90, 607–618.

Corfu, F., 2004. U–Pb geochronology of the Lekres Group: an exotic Early Caledonian metasedimentary assemblage stranded on Lofoten basement, northern Norway. J. Geol. Soc. (Lond.) 161, 619–627.

Corfu, F., Andersen, T.B., 2002. U–Pb ages of the Dalsfjord Campus, SW-Norway, and their bearing on the correlation of the allochthonous crystalline segments of the Scandinavian Caledonides. Int. J. Earth Sci. 91, 955–963.

Corfu, F., Evins, P.M., 2002. Late Paleoproterozoic monazite and titanite U–Pb ages in the Archean Suomujäri complex, N Finland. Precambrian Res. 116, 171–181.

Croudace, I.W., Gilligan, J., 1990. Versatile and accurate trace element determinations in iron-rich and other geological samples using X-ray fluorescence analysis. X-ray Spectrom. 19, 117–123.

Croudace, I.W., Thorpe, O.W., 1988. A low dilution, wavelength dispersive X-ray fluorescence procedure for the analysis of archaeological rock artefacts. Archaeometry 30, 227–236.

Dahlquist, J.A., Rapela, C.W., Baldo, E.G., 2005. Petrogenesis of cordierite-bearing S-type granitoids in Sierra de Chepes, Famatinian orogen, Argentina. J. South Am. Earth Sci. 20, 231–251.

Davis, D.W., Blackburn, C.E., Krogh, T.E., 1982. Zircon U–Pb ages from the Wabigoon. Manitou Lakes Region, Wabigoon Subprovince, northwest Ontario. Can. J. Earth Sci. 19, 254–266.

De Paolo, D.J., 1981. Trace elements and isotopic effects of combined wall rock assimilation and fractional crystallization. Earth Planet. Sci. Lett. 53, 189–202.

Demaiffe, D., Hertogen, J., 1981. Rare earth geochemistry and strontium isotopic composition of a massif-type anorthositic charnockitic body: the Hidra massif (Rogaland, SW Norway). Geochim. Cosmochim. Acta 45, 1545–1561.

Dias, G., Leterrier, J., Mendes, A., Simões, P.P., Bertrand, J.M., 1998. U–Pb zircon and monazite geochronology of post- collisional Hercynian granitoids from the Central Iberian Zone (Northern Portugal). Lithos 45, 349–369.

El-Nisr, S., El-Sayed, M., 2002. The role of fractional crystallization and assimilation in the evolution of the zoned Mukhattata pluton, Eastern Desert, Egypt. Chem. Erde 62, 216–236.

Ferreira, N., Iglésias, M., Noronha, F., Pereira, E., Ribeiro, A., Ribeiro, M.L., 1987. Granitóides da zona Centro-Ibérica e seu enquadramento geodinâmico. In: Bea, F., Carmina, A., Gonzalo, J.C., Plaza, M.L., Rodrigues, J.M.L. (Eds.), Geologia de los granitoids y rocas associadas del Macizo Hespérico, Libro Homenagem a L.C.G. Figueirola. Editorial Rueda, Madrid, pp. 37–53.

Foster, M.D., 1960. Interpretation of trioctahedral micas. U.S. Geol. Surv. Prof. Pap. 354B, 1–49.

Fourcade, S., Capdevila, R., Onabadi, A., Martineau, F., 2001. The origin and geodynamic significance of the Alpine cordierite-bearing granitoids of northern Algeria. A combined petrological, mineralogical, geochemical and isotopic (O, H, Sr, Nd) study. Lithos 57, 187–216.

Frank, M.R., Candela, P.A., Piccoli, P.M., 1998. K-feldspar–muscovite–andalusite–quartz–brine phase equilibria: an experimental study at 25 to 60 MPa and 400 to 550 °C. Geochim. Cosmochim. Acta 62 (23/24), 3717–3727.

Frost, B.R., Barnes, C.G., Collins, W.J., Arculus, R.J., Ellis, D.J., Frost, C.D., 2001. A geochemical classification for granitic rocks. J. Petrol. 42, 2033–2048.

Gomes, M.E.P., Neiva, A.M.R., 2005. Geochemistry of granitoids and their minerals from Rebordelo-Agrochão area, northern Portugal. Lithos 81 (1/4), 235–254.

Holtz, F., Barbey, P., 1991. Genesis of peraluminous granites II. Mineralogy and chemistry of the Tourem Complex (North Portugal) sequential melting vs restite unmixing. J. Petrology 32, 959–978.

Icenhower, J., London, D., 1995. An experimental study of element partitioning among biotite, muscovite and coexisting peraluminous silicic melt at 200 MPa (H_2O). Am. Mineral. 80, 1229–1251.

Jaffey, A.H., Flynn, K.F., Glendenin, L.E., Benthey, W.C., Essling, A.M., 1971. Precision measurement of half lives and specific activities of ^{235}U and ^{238}U. Phys. Rev., C Nucl. Phys. 4, 1889–1906.

Kalt, A., Corfu, F., Wijbrans, J.R., 2000. Time calibration of a P–T path from a Variscan high-temperature low-pressure metamorphic complex (Bayerische Wald, Germany) and the detection of inherited monazite. Contrib. Mineral. Petrol. 138, 143–163.

Krogh, T.E., 1973. A low contamination method for hydrothermal decomposition of zircon and extraction of U and Pb for isotopic age determination. Geochim. Cosmochim. Acta 37, 485–494.

Krogh, T.E., 1982. Improved accuracy of U–Pb zircon ages by creation of more concordant systems using an air abrasion technique. Geochim. Cosmochim. Acta 46, 637–649.

Le Bas, M.J., Streckeisen, A.L., 1991. The IUGS systematics of igneous rocks. J. Geol. Soc. (Lond.) 148, 825–833.

London, D., 1992. Phosphorus in S-type magmas: the P_2O_5 content of feldspars from peraluminous granites, pegmatites and rhyolites. Am. Mineral. 77, 126–145.

London, D., Černý, P., Loomis, J.L., Pan, J.L., 1990. Phosphorus in alkali feldspars of rare-element granitic pegmatites. Am. Mineral. 28, 771–786.

London, D., Wolf, M.B., Morgan VI, G.B., Garrido, M.G., 1999. Experimental silicate-phosphate equilibria in peraluminous granite magmas, with a case study of the Albuquerque batholith at Tres Arroyos, Badajoz, Spain. J. Petrol. 40, 215–240.

Long, P.E., Luth, W.C., 1986. Origin of K-feldspar megacrysts in granitic rocks: implications of a partitioning model for barium. Am. Mineral. 71, 367–375.

Ludwig, K.R., 1999. Isoplot/Ex version 2.03. A geochronological toolkit for Microsoft Excel. Berkeley Geochronology under Special Publication, vol. 1. 43 pp.

Miller, C.F., Stoddard, E.F., Bradfish, I.J., Dollase, W.A., 1981. Composition of plutonic muscovite: genetic implications. Can. Mineral. 19, 25–34.

Mittlefehldt, D.W., Miller, C.F., 1983. Geochemistry of the Sweetwater Wash pluton, California: implications for "anomalous" trace element behaviour during differentiation of felsic magmas. Geochim. Cosmochim. Acta 47, 109–124.

Monier, G., Mergoil–Daniel, J., Labernardière, H., 1984. Générations successives de muscovites et feldspaths potassique dans les leucogranites du massif Millevaches (Massif Central Français). Bull. Mineral. 107, 55–68.

Montero, P., Bea, F., 1998. Accurate determination of $^{87}Rb/^{86}Sr$ and $^{147}Sm/^{144}Nd$ by inductively coupled plasma mass spectrometry in isotope geoscience: an alternative to isotope dilution analysis. Anal. Chim. Acta 358, 227–233.

Nachit, H., Razafimahefa, N., Stussi, J.M., Carron, J.P., 1985. Composition chimique des biotites et typologie magmatique des granitoides. C.R. Acad. Sci. Paris 301 (11), 813–818.

Nakamura, Y., Fujimaki, H., Nakamura, N., Tatsumoto, M., McKay, G., Wagstaff, J., 1986. Hf, Zr and REE partitioning coefficients between ilmenite and liquid: implications for lunar petrogenesis. Proceedings of the 16th lunar and Planetary Science Conference. J. Geophys. Res., vol. 91, pp. D239–D250. Supplement.

Neiva, A.M.R., 1993. Geochemistry of granites and their minerals from Gerez mountain, northern Portugal. Chem. Erde 53, 227–258.

Neiva, A.M.R., 1998. Geochemistry of highly peraluminous granites and their minerals between Douro and Tamega valleys, northern Portugal. Chem. Erde 58, 161–184.

Neiva, A.M.R., Campos, T.F.C., 1992. Genesis of the zoned granitic pluton of Penamacor–Monsanto, Central Portugal. Mem. Not., Publ. Mus. Lab. Mineral. Geol. Univ. Coimbra 114, 51–68.

Neiva, A.M.R., Gomes, M.E.P., 2001. Diferentes tipos de granitos e seus processos petrogenéticos: granitos hercínicos portugueses. Mem. Acad. Ciênc. Lisb. 31, 53–95.

Nockolds, S.R., 1947. The relation between chemical composition and paragenesis in the biotite micas of igneous rocks. Am. J. Sci. 245, 401–420.

Noronha, F., Ramos, J.M.F., Rebelo, J.A., Ribeiro, A., Ribeiro, M.L., 1981. Essai de corrélation des phases de déformation hercyniennes dans le nord-ouest Péninsulaire. Leidse Geol. Meded. 52, 87–91.

Peccerillo, A., Pinarelli, L., Del Moro, A.B., Rotura, A., 1994. Interaction between mafic and salic magmas in granitoids plutons as inferred from geochemical and Sr–Nd isotopic study of enclaves and host granitoids from Cima d'Aste, Southern Alps, Italy. Per. Mineral. 63, 93–111.

Pereira, M.D., Bea, F., 1994. Cordierite-producing reactions in the Peña Negra Complex, Avila Batholith, Central Spain: the role of cordierite in low-pressure anatexis. Can. Mineral. 32, 763–780.

Pereira, A.J.S.C., Neves, L.J.F., Godinho, M.M., Legoinha, P.F.R., 1993. Índice de distorção, parâmetros celulares e composição química de cordierite de granitóides e corneanas da região de Tondela-Oliveira do Hospital (Portugal Central). Mem. Not., Publ. Mus. Lab. Mineral. Geol. Univ. Coimbra 116, 49–62.

Pinto, M.M.S.C., 2001. Mineralizações uraníferas no Vale de Abrutiga e estudo do impacto ambiental da sua exploração. Unpublished M. Sc. thesis, Univ. Coimbra, 312 pp.

Pinto, M.S., Casquet, C., Ibarrola, E., Corrétge, L.G., Pereira, M.R., 1987. Síntese geocronológica dos granitóides do Maciço Hespérico. In: Bea, F., Carmina, A., Gonzalo, J.C., Plaza, M.L., Rodrigues, J.M.L. (Eds.), Geologia de los granitoids y rocas asociadas del Macizo Hespérico. Libro de Homenagem a L.C.G. Figueirola. Editorial Rueda, Madrid, pp. 69–86.

Pitcher, W.S., 1997. The nature and origin of granite. Chapman & Hall, London. 387 pp.

Portuguese Geological Survey, 1992. Carta geológica de Portugal, Escala 1/500 000, Portugal.

Reavy, R.J., Stephens, W.E., Fallick, A.E., Halliday, A.N., Godinho, M.M., 1991. Geochemical and isotopic constrains on petrogenesis: the Serra da Freita pluton, a typical granite body from the Portuguese Hercynian collision belt. Geol. Soc. Amer. Bull. 103, 392–401.

Schärer, U., 1984. The effect of initial ^{230}Th disequilibrium on young U–Pb ages: the Makalu case, Himalaya. Earth Planet. Sci. Lett. 67, 191–204.

Silva, M.M.V.G., Neiva, A.M.R., 1999/2000. Geochemistry of Hercynian peraluminous granites and their minerals from Carregal do Sal-Nelas-Lagares da Beira area, central Portugal. Chem. Erde 59, 329–349.

Stacey, J.S., Kramers, J.D., 1975. Approximation of terrestrial lead isotope evolution by a two-stage model. Earth Planet. Sci. Lett. 34, 207–226.

Valle Aguado, B., Azevedo, M.R., Schaltegger, U., Catalán, J.R., Nolan, J., 2005. U–Pb zircon and monazite geochronology of Variscan magmatism related to syn-convergence extension in Central Northern Portugal. Lithos 82, 169–184.

Vander Auwera, J., Longhi, J., Duchesne, J.C., 1998. A liquid line of descent of the Jotunite (Hypersthene Monzodiorite) Suite. J. Petrology 39 (3), 439–468.

Vigneresse, J.L., 2004. A new paradigm for granite generation. Trans. R. Soc. Edinb. Earth Sci. 95, 11–22.

Villaseca, C., Barbero, L., 1994. Chemical variability of Al–Ti–Fe–Mg minerals in peraluminous granitoid rocks from Central Spain. Eur. J. Mineral. 6, 670–691.

White, 2003. High temperature applications II: oxygen isotopes as an indicator of assimilation. Geol. 656 Isotope Geochemistry. Lectures 30, 227–231.

Williamson, B.J., Downes, H., Thirlwall, M.F., Beard, A., 1997. Geochemical constrains or restite composition and unmixing in the Velay anatectic granite, French Massif Central. Lithos 40, 295–319.

Winter, J., 2001. An Introduction to Igneous and Metamorphic Petrology. Prentice Hall. 697 pp.

York, D., 1969. Least-squares fitting of a straight line with correlated error. Earth Planet. Sci. Lett. 5, 320–324.

Yurimoto, H., Duke, E.F., Papike, J.J., Shearer, C.K., 1990. Are discontinuous chondrite-normalized REE patterns in pegmatitic granitic systems the results of monazite fractionation? Geochim. Cosmochim. Acta 54, 2141–2145.